Websites:
http://www.lifesciencesite.com
http://www.sciencepub.net

Emails:
editor@sciencepub.net
sciencepub@gmail.com

MARSLAND PRESS
Multidisciplinary Academic Journal Publisher

Shear behaviour of reinforced lightweight concrete T-beams

Hesham A. Amna[1], Wael M. Monstaser[2]

[1]- Research Assistant, Structural Engineering Department, Ain Shams University, Cairo, Egypt.
[2]-Assistant Professor, Construction and Building Dept., October 6 University, Giza, Egypt.
wmontaser.eng@o6u.edu.eg

Abstract: An experimental and numerical study was carried out to investigate the validity of using lightweight concrete beams. This study investigated the shear behaviour of lightweight concrete. In this respect, six lightweight concrete beams were tested in two-point bending to study the effect of flange width and shear span to depth ratio. The tests included five beam specimens with a flange and one control beam specimen without a flange. All beams were 120 mm wide and 300 mm tall and had a total length of 2400 mm that was simply supported with a 2000 mm clear span. The beams represented two groups: G1 and G2. The first group consisted of 4 beams, one rectangular section with a cross section of 120 mm x 300 mm and three beams with a T-shaped cross section and flange thickness of 50 mm with varied flange widths of 320 mm, 520 mm and 720 mm. The second group consisted of 2 beams with a flange thickness of 50 mm and a flange width of 520 mm. The details of the specimen material properties, instrumentation, test apparatuses, and testing procedures are presented in this paper. The effect of the studied variables is presented and discussed.
[Hesham A. Amna, Wael M. Monstase. **Shear behaviour of reinforced lightweight concrete T-beams.** *Life Sci J* 2019;16(8):11-27]. ISSN: 1097-8135 (Print) / ISSN: 2372-613X (Online). http://www.lifesciencesite.com. 2. doi:10.7537/marslsj160819.02.

Keywords: Concrete, Beam, Foamed concrete, Lightweight, Shear behaviour, Flange width.

Highlights

- Shear failure in lightweight concrete beams is similar to the shear behaviour of normal weight concrete beams.
- The effect of the flange width and the shear span to depth ratio on the shear behaviour of lightweight concrete beams.

1. Introduction

Structural LWC mixtures can be designed to achieve strengths similar to those of LWC. Structural LWC provides a strength-to-weight ratio in structural elements that is more efficient than that of LWC mixes. In most cases, although the cost of the LWC is little higher than NWC but the reduction in dimension of structural elements, foundations and steel used results in overall lower cost. Furthermore, Lower weight of buildings will reduce the lateral load caused by earthquakes, hence reducing the dimensions and cost of the lateral load carrying system.

In the last 15 years, many researchers aimed to develop structurally and economically efficient LWC and establishing design guidelines for all types of structural elements made using LWC. The resulting concrete mix has a dry unit weight of 18.00 kN/m3, which is in agreement with the technical definition of LWC.

1 Previous Research on the innovative concrete mix

Numerous research programmes have been carried out at the Faculty of Engineering of Ain Shams University to study the properties of the mix in terms of both its material and structural properties.

Okail, H. O. cast six medium-scale reinforced LWC beams and tested them in four-point bending to determine the flexure behaviour of reinforced LWC. Three main parameters were investigated in that study, namely, the flexure reinforcement ratio, concrete type and number of stirrups located in the constant moment zone. The results showed that the beneficial effect of LWC in reducing the members' self-weight triggered only minimal structural disadvantages; the slightly reduced pre-cracking stiffness gradually decreases after cracking until failure, and ductility is reduced. Second, it was found that although increasing the flexural reinforcement ratio logically results in the enhanced flexural capacity of the tested beams, the maximum ratio of reinforcement in the concrete section of ECP-203 is no longer valid for LWC beams because over-reinforcement occurred in beams with a reinforcement ratio less than the maximum. Finally, the previous disadvantages were found to be partially compensated for by the increase in the number of stirrups, inevitably resulting in a slightly increased ductility due to the additional confinement provided to the concrete in compression [1].

Maree, A.F. carried out an experimental programme to investigate the bond behaviour of LWC.

The programme consisted of two phases. It was found that the slippage of the LWC was more than NWC, which also increased slightly with increasing bar diameter. The bond stress ratios of the LWC specimens were found to be greater than those of the NWC because of the higher tensile strength of the LWC. However, the bond stress ratio corresponding to a 0.1 mm slippage of the LWC was lower than that of the NWC. This stress reduction could be attributed to the lower elastic modulus of the LWC in comparison to that of the NWC [2].

El Khouly, S. A. also fabricated an experimental programme to study the time-dependent behaviour of LWC with polystyrene foam particles. The experimental programme consisted of two phases: study of the LWC mechanical properties and the LWC time-dependent behaviour. The results showed that the tested LWC with polystyrene foam particles exhibited a significantly greater drying shrinkage than that of NWC by approximately 31%. The LWC with polystyrene foam particles and NWC with an equal compressive strength were recorded as having equal creep strains during the test period. Generally, the time-dependent strain (shrinkage plus creep) of the LWC with polystyrene foam particles under sustained compressive load was found to be greater than that of NWC with the same compressive strength by approximately9%. The creep strain of the LWC with polystyrene foam particles seemed to be proportional to its stress to strength ratio. The time-dependent deflections of the LWC with polystyrene foam particle beams were greater than those of the NWC beams by approximately 25%. Hence, the time-dependent behaviour of the LWC with polystyrene foam particles in compression and flexure were approximately the same as that of the NWC. The addition of compression steel reinforcement (As`) to the LWC with polystyrene foam particle beams reduced the time-dependent deflections. The sustained load level and LWC time-dependent deflection were directly proportional [3].

1 Experimental Programme

1.1 Details of the tested beams

Six LWC beams were identified as (B1) to (B6): five beam specimens with a flange and one control beam specimen without a flange. All the beams had a total length of 2400 mm that was simply supported with a 2000 mm clear span and 200 mm projection at each end. Additionally, the beams had widths of 120 mm and heights of 300 mm. To study the shear behaviour of LWC, all beams were designed to prevent flexural failure of the beam before shear failure reached. The details of the test specimens are shown in **Error! Reference source not found.**and

Table 1.

Table 1: Details of specimens:

Beam	Breadth (b)	Height (t)	Flange thickness (ts)	Flange width (B)		B/b	Span to depth ratio (a/d)
Specimen	mm	mm	mm	--	mm	--	--
B1	120	300	--	b	120	1	3
B2	120	300	50	b+4ts	320	2.67	3
B3	120	300	50	b+8ts	520	4.3	3
B4	120	300	50	b+12ts	720	6	3
B5	120	300	50	b+8ts	520	4.3	1.8
B6	120	300	50	b+8ts	520	4.3	3.6

1.2 Material properties

1.2.1 Concrete

1.2.1.1 Mix Proportion of Lightweight Concrete

Numerous trial batches were developed at the materials laboratory of the faculty of engineering, Ain Shams University, to achieve a LWC with a considerable difference in weight but approximately the same compressive strength as those of NWC. The design proportions for the mix are shown in

Table 2: Material quantities of the LWC specimens:

	Cement (kg/m^3)	Silica Fume (kg/m^3)	Coarse Aggregate (kg/m^3)	Sand (kg/m^3)	Polystyrene Foam (litre/m^3)	Super Plasticizer (litre/m^3)	w/c ratio	Target Concrete Strength (MPa)
LWC	450	40	630	630	330	13.5	0.308	30

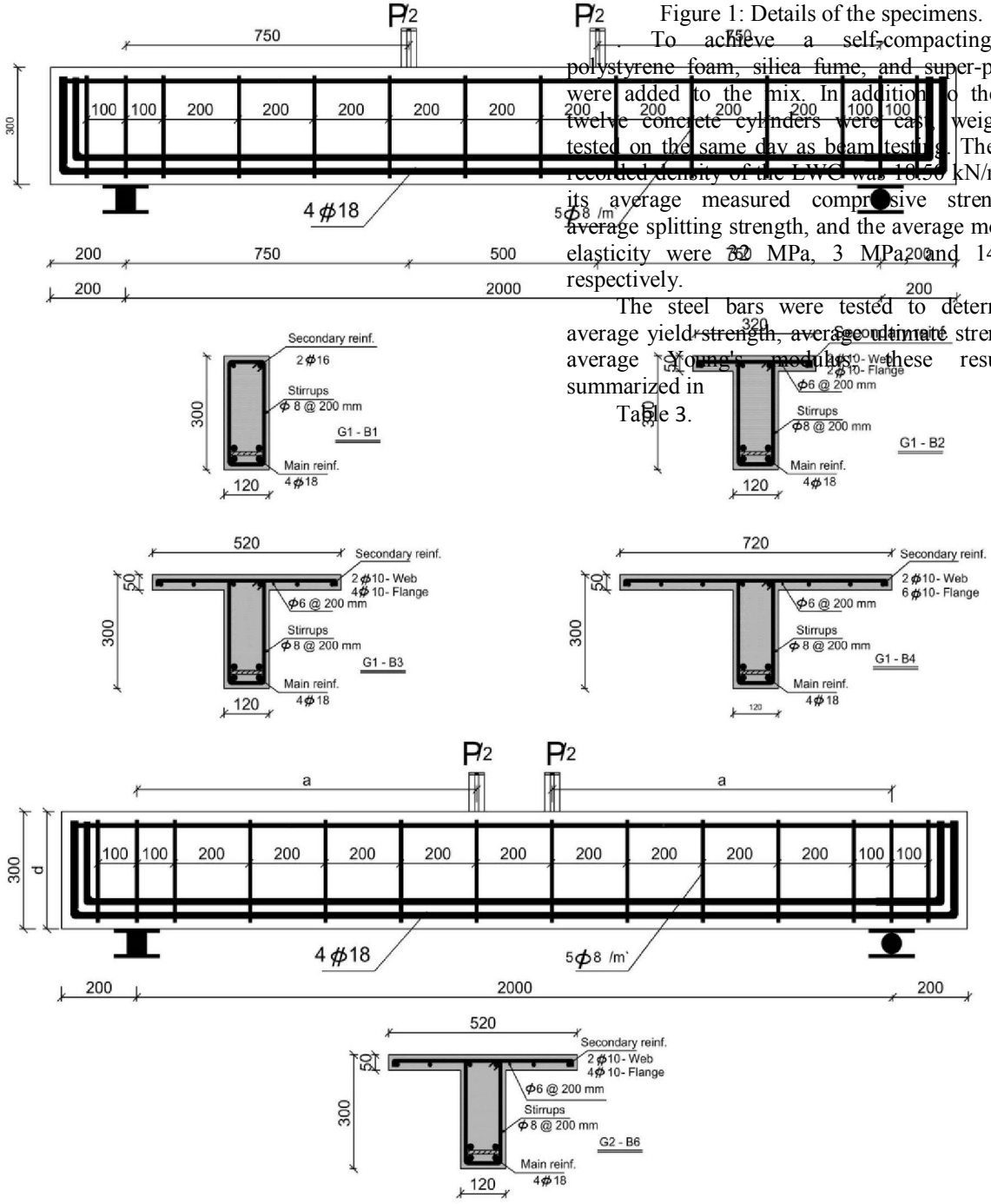

Figure 1: Details of the specimens.

To achieve a self-compacting LWC, polystyrene foam, silica fume, and super-plasticizer were added to the mix. In addition to the beams, twelve concrete cylinders were cast, weighed and tested on the same day as beam testing. The average recorded density of the LWC was 18.50 kN/m^3, while its average measured compressive strength, the average splitting strength, and the average modulus of elasticity were 32 MPa, 3 MPa, and 14.0 GPa, respectively.

The steel bars were tested to determine the average yield strength, average ultimate strength, and average Young's modulus; these results are summarized in Table 3.

no.	Beam	b	t	ts	Flange width (B)	B/b	Span to depth ration (a/d)	Group
	Specimen	mm	mm	mm	mm	-	-	-
3	B3	120	300	50	520	4.3	3	G2
5	B5	120	300	50	520	4.3	1.8	G2
6	B6	120	300	50	520	4.3	3.6	G2

Table 2: Material quantities of the LWC specimens:

	Cement (kg/m^3)	Silica Fume (kg/m^3)	Coarse Aggregate (kg/m^3)	Sand (kg/m^3)	Polystyrene Foam ($litre/m^3$)	Super Plasticizer ($litre/m^3$)	w/c ratio	Target Concrete Strength (MPa)
LWC	450	40	630	630	330	13.5	0.308	30

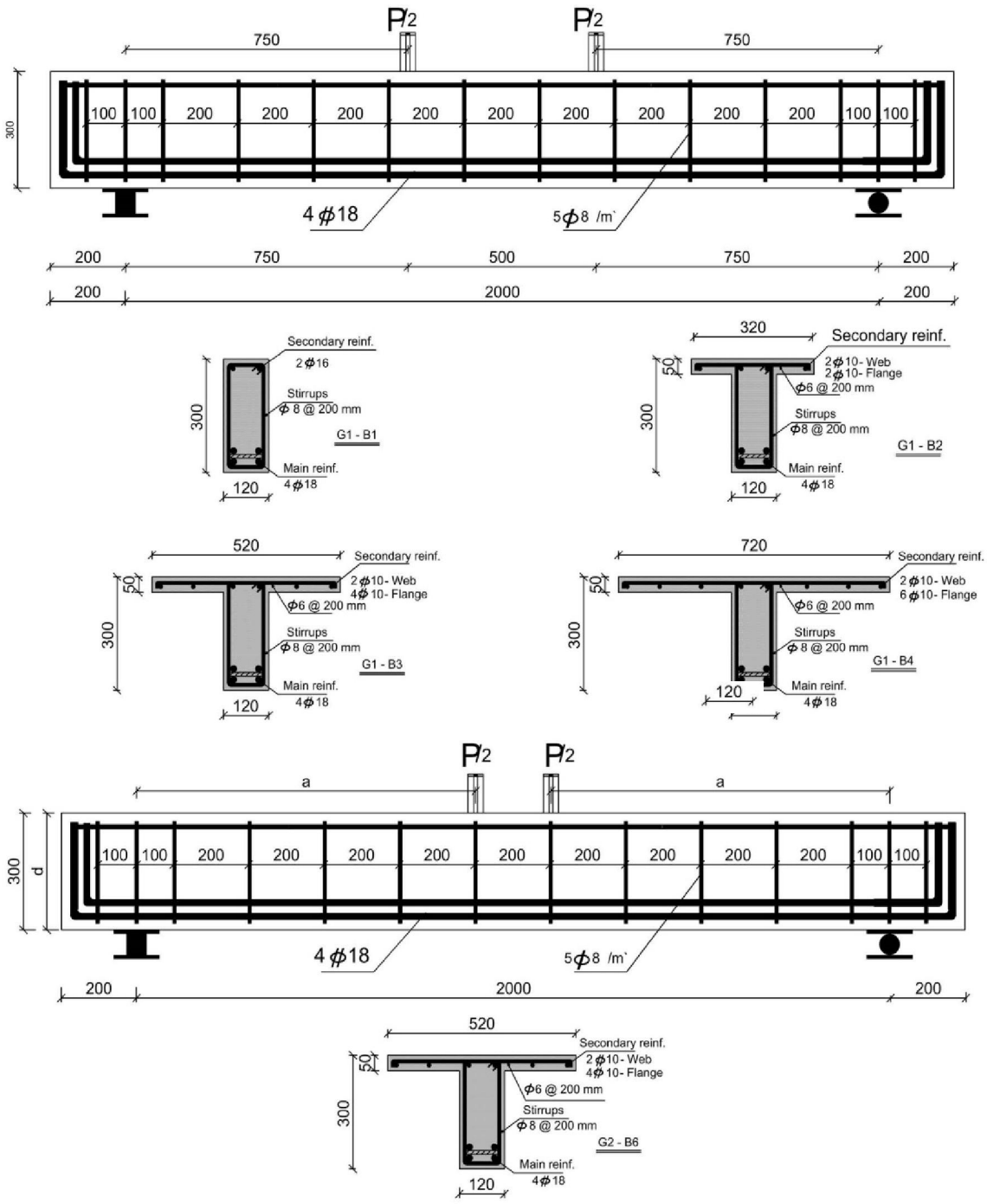

no.	Beam	b	t	ts	Flange width (B)	B/b	Span to depth ration (a/d)	Group
	Specimen	mm	mm	mm	mm	-	-	-
3	B3	120	300	50	520	4.3	3	G2
5	B5	120	300	50	520	4.3	1.8	G2
6	B6	120	300	50	520	4.3	3.6	G2

Figure 1: Details of the specimens.

Table 3: Mechanical properties of the tested steel:

	Diameters Used (mm)	Average Young's Modulus (MPa)	Average Yield Strength (MPa)	Average Ultimate Strength (MPa)
Mild Steel	6 & 8	2E+005	380	540
High Tensile Steel	10	1.8E+005	470	690
	16 & 18	1.8E+005	490	705

1.3 Test procedure

Two sides of each specimen were painted white to facilitate the tracing of cracks during tests. The specimens were incrementally loaded until failure. The tested specimens were instrumented to measure their deformational behaviour after each load increment was applied. Strain gauges were attached on the concrete surface to measure the concrete strain in the compression zone during testing as shown in Figure 2.

2 Nonlinear Finite Element Analysis Using ANSYS®

2.1 Introduction

FE analyses using ANSYS®[4] used to study the structural behaviour of reinforced concrete members. All structural elements can be studied using ANSYS. In general, good analytical results have been obtained for such elements when compared to experimental results, mostly when compared to global load-deformation curves, crack patterns and stress distributions[5][6][7]. For the purposes of this paper, the shear behaviour of concrete elements was modelled in ANSYS®.

2.2 Element types used for modelling

The Solid65 element [8] was used to model the concrete elements. This element has eight nodes with three degrees of freedom per node (translations in the nodal x, y, and z directions), and it is capable of plastic deformation, cracking and crushing in three orthogonal directions (Figure 3a, Table 4). To apply a discrete model, the Link180 element [8] was used to model the steel reinforcement (Figure 3b, Table 5). This element is a 3-D spar element and has two nodes, each with three degrees of freedom.

The Solid 185 element [8] was used to model the steel plate elements (Figure 3c, Table 6).

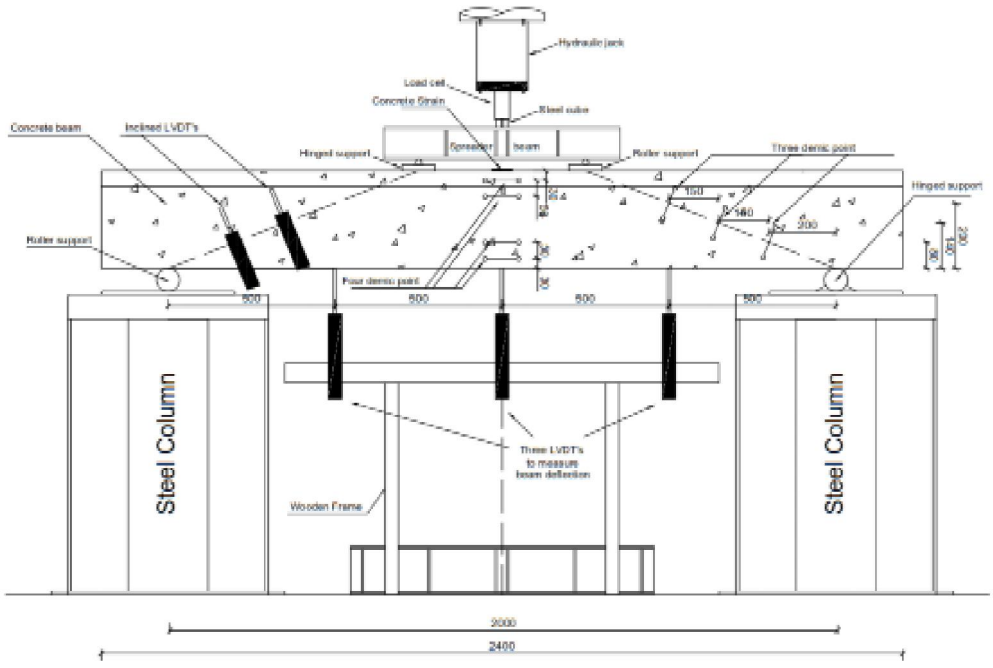

Figure 2: Test setup.

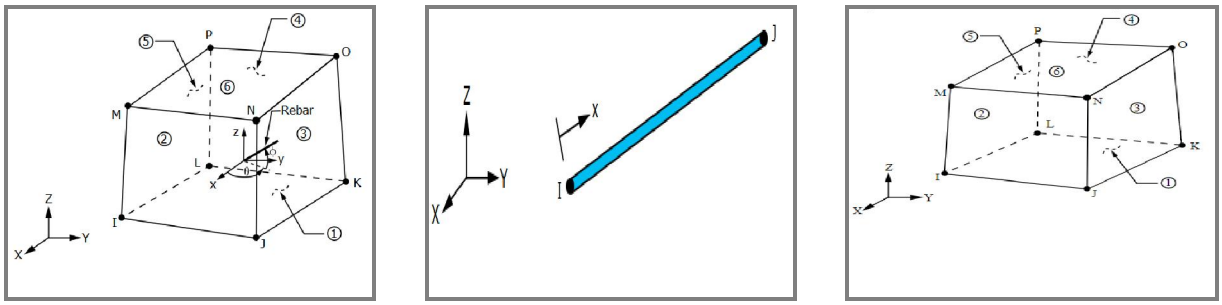

(a): SOLID65 element (b): LINK180 element (c): SOLID185 element

Figure 3: Element types used for modelling.

Table 4: Material properties of the concrete elements:

Material Model No.	Element Type	Material Properties							
		Density N/mm^3	Linear Isotropic		Multi linear Isotropic			Concrete	
					Point No.	Stress	Strain		
1	SOLID65	1.8E-005	EX	14.00 GPA	Point 01	0.000558	7.8	Open Shear Transfer Coef.	0.3
					Point 02	0.00126	14.867	Closed Shear Transfer Coef.	0.9
					Point 03	0.00137	15.911	Uniaxial Cracking Stress	3
					Point 04	0.00165	17.975	Uniaxial Crushing Stress	26.5
					Point 05	0.0024	22.109	Biaxial Crushing Stress	0
			PRXY	0.18	Point 06	0.00302	24.111	Hydrostatic Pressure	0
					Point 07	0.00368	25.615	Hydro Biax. Crush Stress	0
					Point 08	0.00385	25.812	Hydro Uniax. Crush Stress	0
					Point 09	0.0042	26.152	Tensile Crack Factor	0.6

Table 4: Material properties of the steel reinforcement elements:

Material Model No.	Diameter	Element Type	Material Properties				
			Density	Linear Isotropic		Bilinear Isotropic	
				EX	PRXY	Tang Stss	Tang Mod
2	18	LINK180	7.85E-005	1.8E+005	0.3	490	200
3	16	LINK180		1.8E+005	0.3	490	200
4	10	LINK180		1.8E+005	0.3	470	200
5	8	LINK180		2E+005	0.3	400	200
6	6	LINK180		2E+005	0.3	400	200

Table 5: Material properties of the steel plate elements:

Material Model No.	Element Type	Material Properties				
		Density	Linear Isotropic		Bilinear Isotropic	
			EX	PRXY	Tang Stss	Tang Mod
7	SOLID185	7.85E-005	2E+005	0.3	--	--

3 Experimental Results

3.1 Failure mode

- In the experiments, the failure load of each beam increased with the flange width; for flange widths of 320 mm, 520, and 720 mm, the failure load was greater than that of the rectangular beam by approximately 10%, 15%, and 18%, respectively.
- In the experiments, the moment cracking load force ranged from 60 to 70 kN, and the values were approximately 33.3 to 34.6% of the failure load. The table of results show the difference between the control beam and the beams with various flange widths; however, the beams with different upper flange widths have the same moment cracking load. This difference was attributed to the presence of the upper flange in (B2), (B3), and (B4), increasing the stiffness of the beam section.
- In the experiments, the shear cracking load force ranged from 70 to 80 kN, approximately 38 to 41% of the failure load. The table of results shows the difference between the control beam and the beams with different flange widths; however, the beams with different upper flange widths have the same shear cracking load. This difference was attributed to the presence of the upper flange in (B2), (B3), and (B4), which increases the stiffness of the beam section and increases the shear capacity of the section with different ratios.
- No significant difference in the ultimate shear carrying capacity of the beam specimens (B2), (B3), and (B4) was observed. However, their ultimate shear carrying capacities are greater than that of (B1), which is a rectangular beam. The beam specimens (B3) and (B4) have very similar shear failure load values, as illustrated in the figures below.
- The failure load of (B5) increased by 15.5% due to a decrease in the shear span to depth ratio from 3.0 to 1.8.
- The failure load of (B6) decreased by 10% due to an increase in the shear span to depth ratio from 3.0 to 3.6.
- The failure load differed with the variation in the shear span to depth ratio; the failure load was approximately 90 to 115% of that of the control beam from the previous group (B3).
- The moment cracking load force increased to 110 kN due to a decrease in thee shear span to depth ratio from 3.0 to 1.8 and decreased to 60 kN with an increase in the shear span to depth ratio from 3.0 to 3.6.
- The shear cracking load force increased to 90 kN due to a decrease in the shear span to depth ratio from 3.0 to 1.8 and decreased to 70 kN with an increase in the shear span to depth ratio from 3.0 to 3.6.
- A significant increase in the ultimate shear carrying capacity with decreasing shear span to depth ratio was observed.
- All beams failed in shear before flexural capacity was reached; no slip of the flexural capacity is reached, and no slip of flexural reinforcement was observed during the beam tests.

3.2 Cracking pattern

It was observed that all the beams have similar characteristics of crack formation. The crack formation was initiated in the flexural span between the two concentrated loads where the highest flexural stress and zero shear stress. The cracks were perpendicular to the direction of the maximum principal tensile stress induced by pure bending. As the load increased, additional flexural cracks started within the shear zone. Due to the effect of a combined shear and bending stress, the existing flexural cracks extended into flexure-shear cracks. With increasing load, additional shear cracks formed in the shear span between the locations of the applied load and the support. Then, because of the dominance of the shear stresses, the cracks became progressively more inclined and propagated towards the load points, ultimately leading to shear failure as shown in Figure.

Table 6shows that shear cracking initiated after flexural cracking in all the beam specimens. All of the cracks were marked at each load level during the test, up to the failure load level.

Table 6: Summary of the test results for the beam specimens:

Beam	Flange width (B)		B/b	Shear span to depth ratio (a/d)	Moment cracking load	Shear cracking load	Failure load
Specimen	--	mm	-	-	kN	kN	kN
B1	b	120	1	3	60	70	173
B2	b+4ts	320	2.67	3	70	80	190
B3	b+8ts	520	4.3	3	70	80	200
B4	b+12ts	720	6	3	70	80	205
B5	b+8ts	520	4.3	1.8	110	90	231
B6	b+8ts	520	4.3	3.6	60	70	181

3.3 Load-deflection response

The first parts of the load-deflection plots, to flexural cracking, for each beam were similar and represent the behaviour of the un-cracked beam's section, utilizing the gross moment of inertia of the concrete cross section. In this part of the plot, the load-deflection relationship was linear. The second part of the plot, after cracking and to failure, represents the cracked beam with a reduced moment of inertia.

For the load-deflection relationship shown in Figure 5a, the maximum deflection of the beam specimens was measured at the mid-span of the specimen. Deflection was also measured at different locations, as mentioned in section3. It was found that deflections in the fallen half were greater than those in the second half.

There is a significant decrease in the deflection of (B2), (B3), and (B4) compared with the control beam (B1), possibly attributable to the presence of the flange (high stiffness of the T-section). In addition, there is a difference in the resultant deflection between (B2) and (B3). This may be attributed to the flange width variance. Finally, there is no remarkable decrease in deflection from (B3) and (B4). This may be attributed to the increase in the flange width of more than (bw+8ts), which has a negligible effect on the deflection, as shown in Figure 5a.

As shown in Figure 5b, the load-deflection relationship of beam specimens (B3) and (B6) exhibited similar characteristics, but it can be seen from the load-deflection relationship that the beam specimens (B3) and (B6) have similar curves in the early loading process. They then separate significantly until the failure load for each beam specimen is reached, with more deflection for (B6) than (B3), where (B3) provides a higher shear carrying capacity and lower deflection than those of (B6). Additionally, Figure 6shows a significant increase in the ultimate shear carrying capacity and a significant decrease in the deflection for beam specimen (B5) over beam specimens (B3) and (B6).

Figure 4: Crack patterns in the beams.

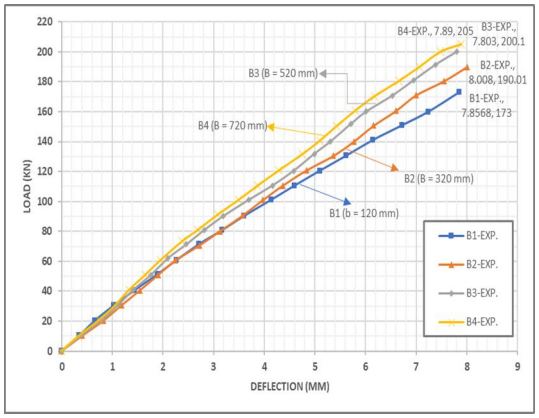

(a) B1 & B2 & B3 & B4

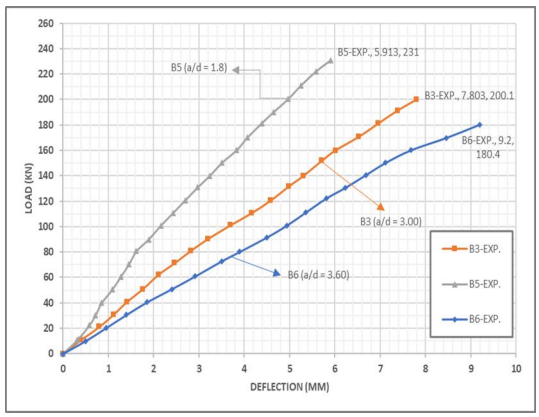

(b) B3 & B5 & B6

Figure 5: Applied load versus deflection of the experimental results.

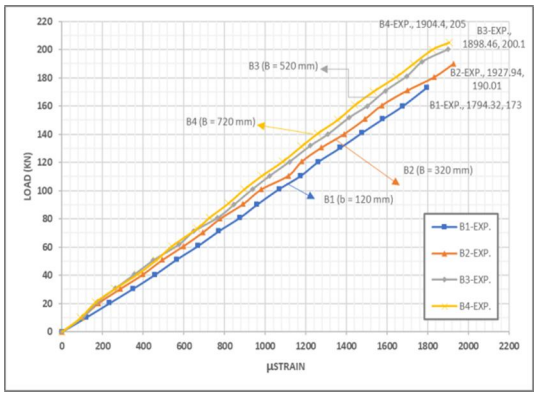

(a) B1 & B2 & B3 & B4

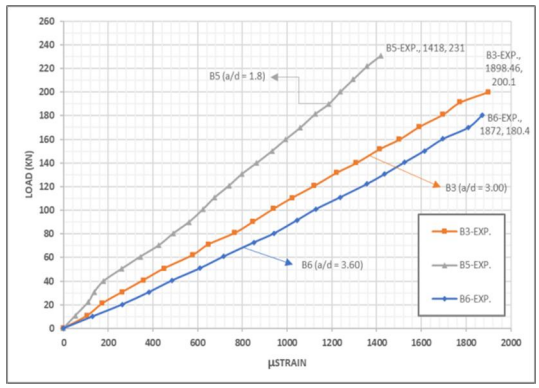

(b) B3 & B5 & B6

Figure 6: Applied load versus longitudinal steel strain of the experimental results.

3.4 Longitudinal steel strain

For the first four beams tested, the load-steel strain relationship seems to be linear. The maximum tensile strain in the flexural reinforcement ranged between 1795 με and 1905 με. Figure 6a shows that there is a small decrease in the main steel strain, which is inversely proportional to the increase in flange width. This may be attributed to the presence of the flange width (high stiffness of the T-section); consequently, the dowel shear resistance was decreased.

For (B5) and (B6), the load-steel strain relationship seems to be linear. The maximum tensile strain in the flexural reinforcement ranged between 1418 με and 1872 με. As observed in Figure 6b, it is clear that decreasing the shear span to depth ratio (a/d) significantly reduces the steel strain.

All beam specimens (B5, B3 & B6) were designed to prevent premature flexural failure. Because all the beams have the same inertia and reinforcement, the moment and the longitudinal strain of the steel in the beams are approximately equal, and there is no significant difference in the longitudinal steel strain values for the same moment, as shown in Figure 7.

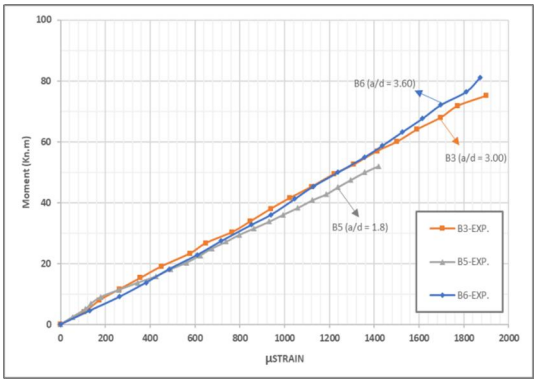

Figure 7: Applied moment versus longitudinal steel strain for beam specimens (B3), (B5), and (B6).

3.5 Stirrup steel strain

For beam specimens (B1), (B2), (B3) and (B4), which failed in the shear zone after the stirrups yielded, as shown in Figure 8a, the load-strain relationships were similar, and there is clearly no significant difference in the strain among all the beams

as the stirrups yielded. Additionally, the load-strain plot shows that the stirrup strain was greater for (B1) than for (B2) and that the stirrup strain for (B2) was higher than that for (B3), but the plots for beam specimens (B3) and (B4) are similar. There is a small decrease in stirrup steel strain that is inversely proportional to that increase in flange width. This result may be attributed to the presence of the flange (high stiffness of the T-section).

For beam specimens (B3), (B5) and (B6), which failed in the shear zone after the stirrups yielded, as shown in Figure 8b, the load-strain relationships exhibited similar behaviours, and the stirrup strains of (B3) and (B6) were similar. The plots also show that the yielding of the stirrups in (B3) and (B6) begun nearly at the same load level, but for (B5), the yielding began after greater load levels were applied. The increase in stirrup steel strain is directly proportional to the increase in the shear span to depth ratio.

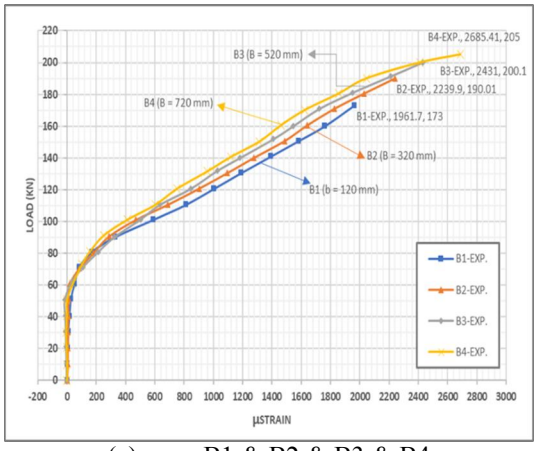

(a) B1 & B2 & B3 & B4

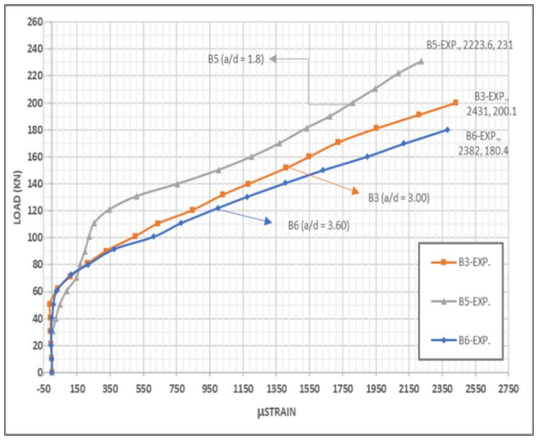

(b) B3 & B5 & B6

Figure 8: Applied load versus stirrup steel strain of the experimental results.

3.6 Concrete strain

A comparison of the concrete strain of specimens (B2), (B3), and (B4) with that of the control beam (B1) shows that there is a significant decrease in the concrete strain of (B2), (B3), and (B4) compared with that of the control beam (B1). This may be attributed to the presence of the flange. In addition, there is a difference in concrete strain between specimens (B2) and (B3), possibly attributable to the flange width variance. Finally, there is no remarkable decrease in deflection between (B3) and (B4), possibly attributable to the increase in the flange width above (b_w+8t_s), which has a negligible effect on the concrete strain of the tested beams. Figure 9a shows the relation between the applied load and the concrete strain for the first group of specimens.

For beam specimens (B2), (B3), and (B4), which have a shear span to depth ratio of a/d=3.00 and flange widths bw+4ts = 320 mm, bw+8ts = 520 mm, bw+12ts = 720 mm, respectively, it was found that the compressive concrete strain decreased by approximately 23.6%, 41.6%, and 43.9%, respectively, from that of specimen (B1) with a rectangular section, at the load of 170 kN.

Regarding beam specimens (B3), (B5) and (B6), which have the same flange width but varied shear span to depth ratios, there is a significant increase in concrete strain in the compression zone for specimen (B6) compared to specimen (B5), and the concrete strain in specimen (B3) plots between them. In brief, there was a noticeable increase in concrete strain that was directly proportional to the increase in the shear span to depth ratio. Figure 9b shows the relation between the applied load and the concrete strain for the second group of specimens.

Regarding beam specimens with the same flange width of 520 mm, for (B5), which has a/d=1.8, the stirrup steel strain decreased by approximately 38.4% from that of (B3), which has a shear span to depth ratio equal to a/d=3.0 at the same load level of 170 kN.

For beam (B6), which has a/d=3.6, the stirrup steel strain increased by approximately 68.1% from that of (B3), which has a shear span to depth ratio equal to a/d=3.0 at the same load level of 170 kN.

4 Nonlinear Finite Element Analysis Results

The following subsections discuss the results of the numerical investigation using nonlinear FE analysis after verification with the experimental results data for the six tested beams.

In the NLFEA, the specimens were analysed for loads from zero to the failure load, in equal increments. The prescribed FE models were validated against the results of the six tested beams. The predicted load carrying capacity and failure mode for each specimen were carefully examined against the

test results. The FE results, including plots of the mid-span deflection, steel strain, stirrup strain and concrete strain for each of the models, are presented. The graphs are presented at certain critical points, where the maximum values are expected to occur. To verify the FEM, a comparison of the results obtained from the tests and from the FEA is presented in the following sections.

4.1 Cracking and ultimate loads

Table 7 shows the moment cracking load, shear cracking load, and failure load obtained from the experimental programme and the corresponding FEM predictions for the beams. The ultimate loads obtained from the FEA represent the load levels at which the model failed to reach convergence, which means that either the concrete or the steel strain reached its ultimate value or a stability failure occurred. The last column in Table 7 gives the ratio between the experimental and the FE results for a certain moment cracking load, shear cracking load, and failure load. The results of the failure load show that the average deviation between the experimental and FE results at the ultimate loads were 4.14% with a standard deviation of 1.62%.

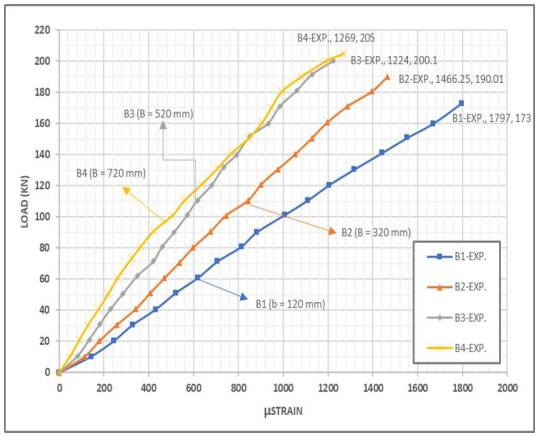

(a) B1 & B2 & B3 & B4

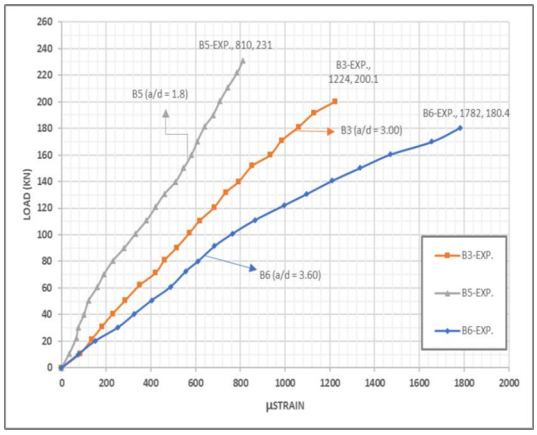

(b) B3 & B5 & B6

Figure 9: Applied load versus concrete compressive strain from the experimental results.

4.2 Crack Pattern

The ANSYS® program records a crack pattern at each applied load step. It shows the development of the cracks. For all beams, early flexural cracks occur in the mid-span. After increasing the applied loads, vertical flexural cracks spread horizontally from the mid-span to the support. At a higher applied load, diagonal tensile cracks appear. Increasing the applied load induces additional diagonal and flexural cracks. Finally, compressive cracks appear at nearly the last applied load step; these cracks appear near the loading location.

The first cracking load for all beams was between 45 kN and 80 kN. The cracking load was not determined accurately because the load increment remained constant during the entire analysis. The experimental first cracking load was between 60 kN and 110 kN, which agrees with the FE results.

4.3 Load-deflection behaviour

The deflections of the beams were also measured using the FE program (ANSYS®). The applied load versus mid-span deflection relationships for the tested beams is presented in Figure 11.

A comparison of the load-deflection results between the FEA and experiments shows that the first zone of the load-deflection curves is a linear zone up to the first flexural cracking load. The second zone is a posted flexural cracking zone that represents the initiation, spreading, and widening of inclined shear cracks until failure. Additionally, we noticed that the FEA load-deflection curves reflect stiffness slightly stiffer than those of the experimental load-deflection curves, although the FEA curves show good agreement with the experimental findings.

Additionally,

Table 8shows the maximum deflection values achieved at the same load level in the experimental and FE tests. Notably, 170 kN was used as a fixed load level for comparison of the deflection of all the beams. The table illustrates the ratio of the deflection values between the FE results and the experimental results at a fixed load of 170 kN. The results show that the deviation between the experimental results and FE results for all beams is 7.02% with a standard deviation of 4.18%.

4.4 Longitudinal steel strain

Table 10,12shows a comparison of the longitudinal steel strain between the experimental and FE results at a load of 170 kN and at failure load, and Figure 12 shows a comparison of the longitudinal steel strain between the experimental and FE results.

4.5 Stirrup steels train

Table **12**,14shows a comparison of the stirrup steel strain between the experimental and FE results at a load of 170 kN and at failure load, and **Error! Reference source not found.** shows a comparison of the stirrup steel strain between the experimental and FE results.

4.6 Compressive concrete strain

Error! Reference source not found., 16shows a comparison of the compressive concrete strain between the experimental and FE results at a load of 170 kN and at failure load, and Figure 13shows a comparison of the compressive concrete strain between the experimental and FE results.

Table 7: Comparison of the moment cracking load, shear cracking load, and failure load results between the experiments and FE models.

Beam	Moment cracking load			Shear cracking load			Failure load		
	EXP	FE	(EXP/FE)	EXP	FE	(EXP/FE)	EXP	FE	(EXP/FE)
Specimen	kN		%	kN			kN		%
B1	60	45	133	70	60	116.67	173	182.6	95.05
B2	70	45	155	80	65	123	190	197	96.45
B3	70	50	140	80	65	123	200	210.8	94.79
B4	70	50	140	80	65	123	205	208.3	98.56
B5	110	80	137.5	90	85	105.8	231	247.8	93.52
B6	60	45	133	70	63	111	180.4	186.4	96.79
							Average		95.86%
							Standard Deviation		1.62

FE Crack Pattern

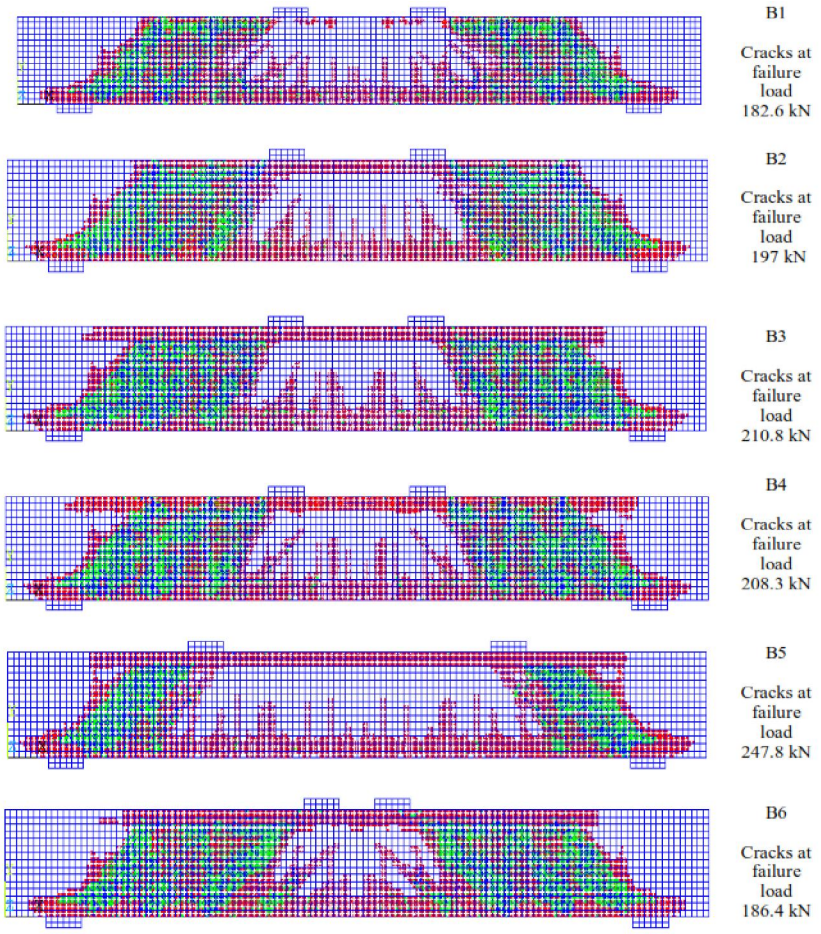

Figure 10: Crack propagation in the beam specimens.

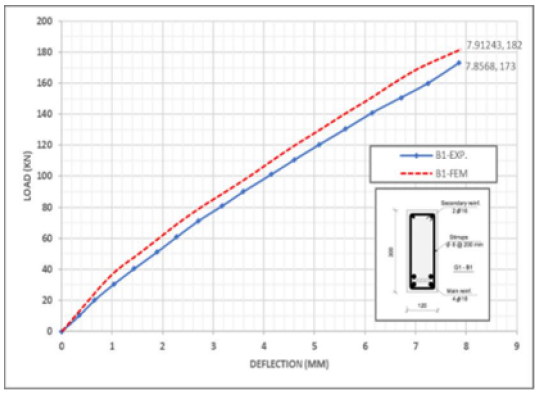

Load-deflection curve for (B1)

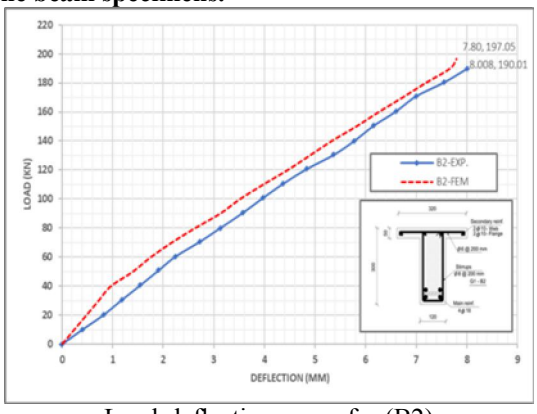

Load-deflection curve for (B2)

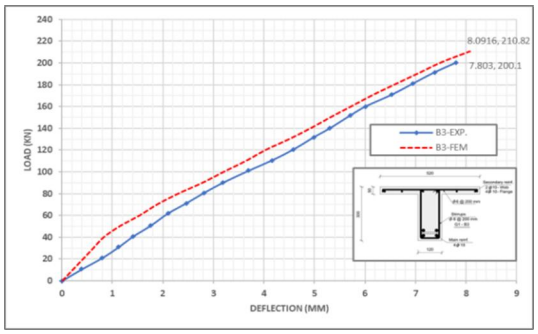

Load-deflection curve for (B3)

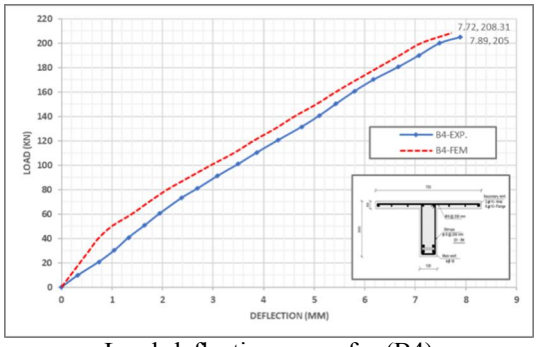

Load-deflection curve for (B4)

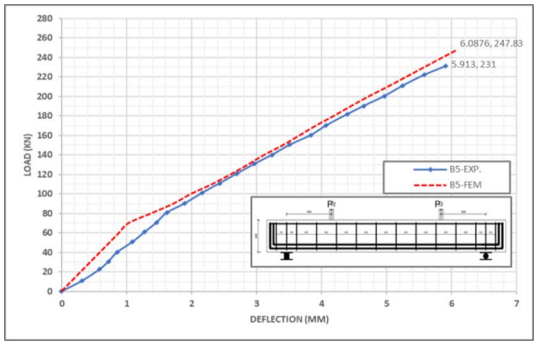

Load-deflection curve for (B5)

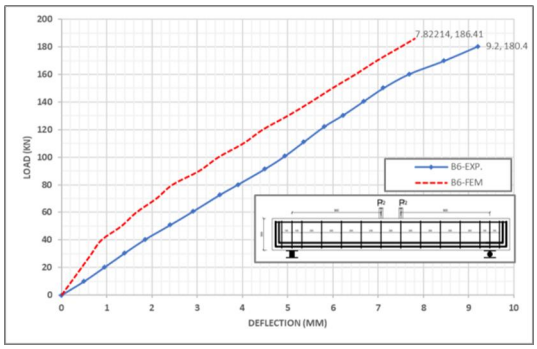

Load-deflection curve for (B6)

Figure 11: Applied load versus deflection of the beam specimens.

Table 8: Comparison of the deflection between the experimental and FE results at a load of 170kN:

Beam		**Deflection at 170 kN**		**(FE/EXP) %**
		EXP	FE	
Specimen		mm		%
B1		7.7	7.1	92.21
B2		6.996	6.732	96.23
B3		6.52	6.15	94.33
B4		6.17	5.84	94.65
B5		4.06	3.91	96.31
B6		8.45	7.11	84.14
Average	92.98			
Standard Deviation	4.18			

Table 9: Comparison of the deflection between the experimental and FE results at the failure load:

Beam	**Experimental Results**		**Finite Element Results**	
	Load	Def.	Load	Def.
Specimen	kN	mm	kN	mm
B1	173	7.856	182.6	7.912
B2	190	8.008	197	7.7996
B3	200	7.803	210.8	8.096
B4	205	7.89	208.3	7.72
B5	231	5.913	247.8	6.087
B6	180.4	9.2	186.4	7.822

Table 10: Comparison of the steel strain between the experimental and FE results at a load of 170kN:

No.	**Beam**	**Longitudinal Steel Strain at 170 kN**		**(FE/EXP) %**
		EXP	FE	

	Specimen	µSTRAIN		%
1	B1	1794	1573	87.68
2	B2	1699	1530	90.05
3	B3	1591	1497	94.09
4	B4	1531	1471	96.08
5	B5	1057	932	88.17
6	B6	1810	1690	93.37
Average	91.58			
Standard Deviation	3.11			

Table 11: Comparison of the longitudinal steel strain between the experimental and FE results at the failure load.

No.	**Beam**	**Experimental Results**		**Finite Element Results**	
		Load	Strain	Load	Strain
	Specimen	kN	µSTRAIN	kN	µSTRAIN
1	B1	173	1794.32	182.6	1688.97
2	B2	190	1927.94	197	1769.92
3	B3	200	1898.46	210.8	1860.18
4	B4	205	1904.4	208.3	1812.48
5	B5	231	1418	247.8	1380.7
6	B6	180.4	1872	186.4	1849.56

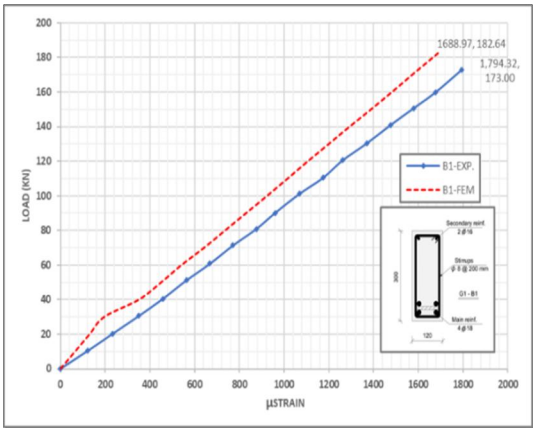

Longitudinal steel strain curve for (B1)

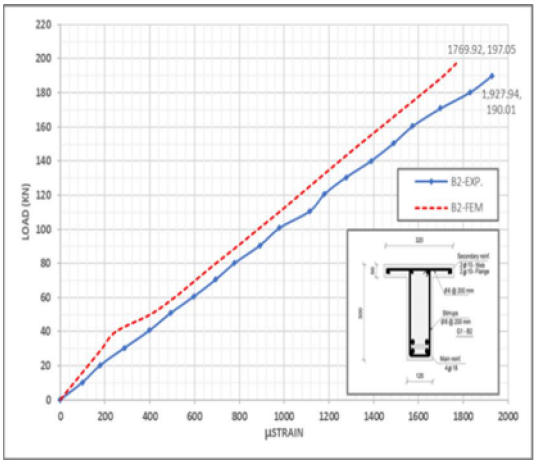

Longitudinal steel strain curve for (B2)

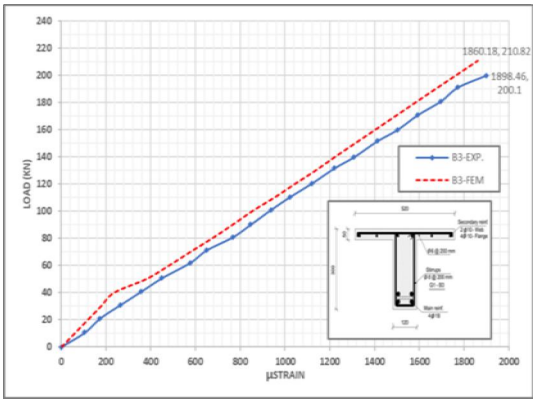

Longitudinal steel strain curve for (B3)

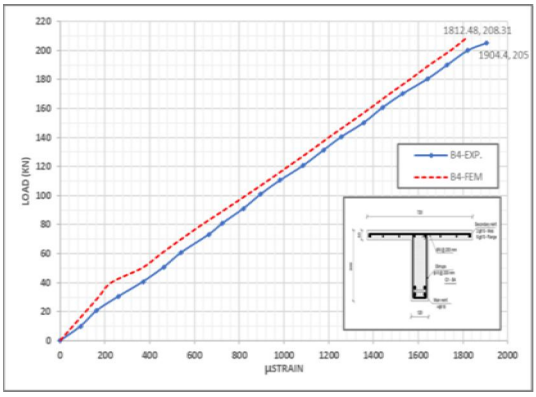

Longitudinal steel strain curve for (B4)

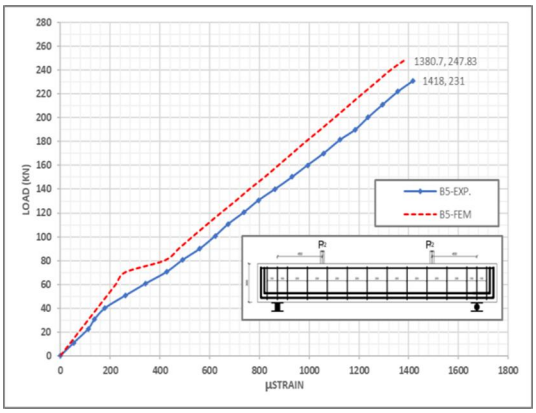

Longitudinal steel strain curve for (B5)

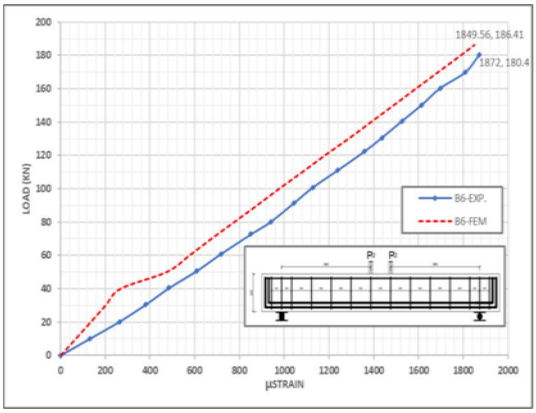

Longitudinal steel strain curve for (B6)

Figure 12: Applied load versus longitudinal steel strain for the beam specimens.

Table 12: Comparison of the steel strain between the experimental and FE results at a load of 170kN:

Beam		Stirrup steel Strain at 170 kN		(FE/EXP) %
		EXP	FE	
Specimen		μSTRAIN		%
B1		1962	1624	82.77
B2		1826	1583	86.69
B3		1723	1567	90.95
B4		1626	1500	92.25
B5		1367	1197	87.56
B6		2119	1599	75.46
Average	85.95			
Standard Deviation	5.6			

Table 13: Comparison of the stirrup steel strain between the experimental and FE results at the failure load.

No.	Beam	Experimental Results		Finite Element Results	
		Load	Strain	Load	Strain
	Specimen	kN	μSTRAIN	kN	μSTRAIN
1	B1	173	1961.7	182.6	1723
2	B2	190	2239.9	197	1850.9
3	B3	200	2431	210.8	2001.26
4	B4	205	2685.41	208.3	2001.43
5	B5	231	2223.6	247.8	1732.9
6	B6	180.4	2382	186.4	1768.24

Table 14: Comparison of the compressive concrete strain between the experimental and FE results at a load of 170kN.

Beam		Compressive Concrete Strain at 170 kN		(EXP/FE) %
		EXP	FE	
Specimen		μSTRAIN		%
B1		1686	1658	101.69
B2		1287	1344	95.76
B3		985	1139	86.48
B4		946	1092	86.63
B5		606	629	96.34
B6		1656	1848	89.61
Average	92.75			
Standard Deviation	5.61			

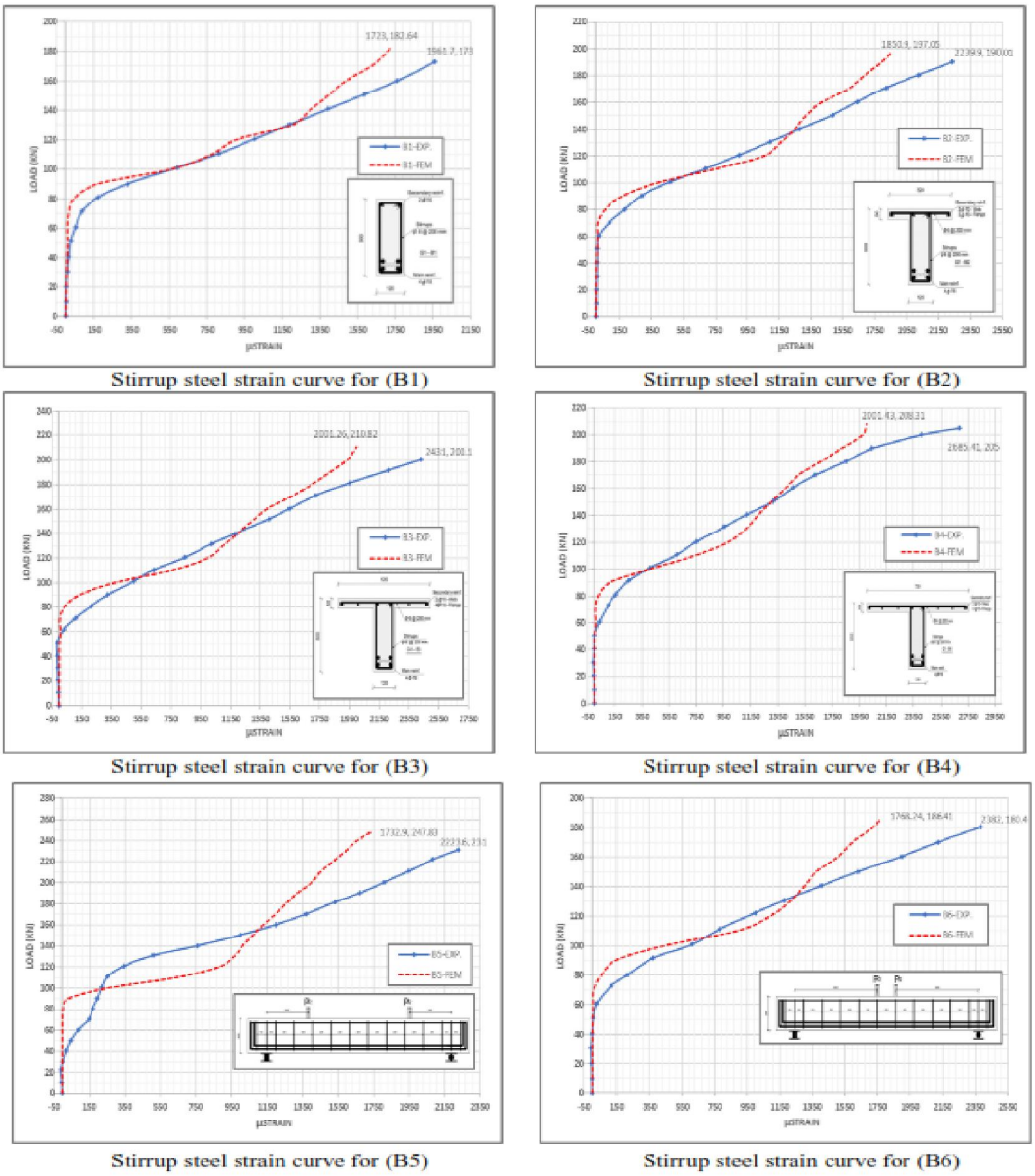

Figure 13: Applied load versus stirrup steel strainin thebeam specimens.

Table 15: Comparison of the compressive concrete strain between the experimental and FE results at the failure load.

No.	Beam	Experimental Results		Finite Element Results	
		Load	Strain	Load	Strain
	Specimen	kN	µSTRAIN	kN	µSTRAIN
1	B1	173	1797	182.6	1760
2	B2	190	1466.25	197	1545.75
3	B3	200	1224	210.8	1418.8
4	B4	205	1269	208.3	1353
5	B5	231	810	247.8	909
6	B6	180.4	1782	186.4	2005

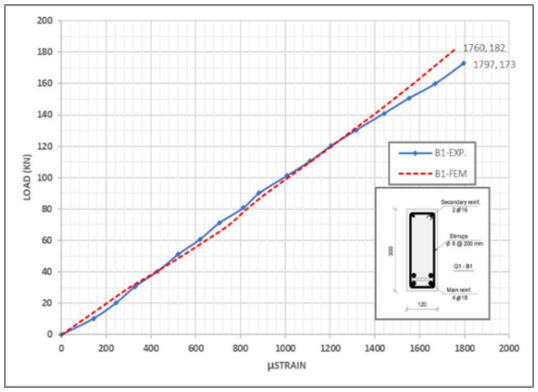

Compressive concrete strain curve for (B1)

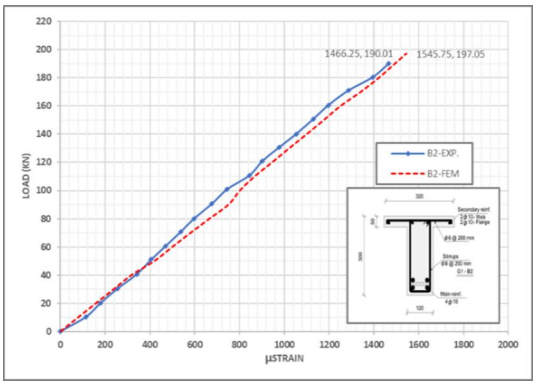

Compressive concrete strain curve for (B2)

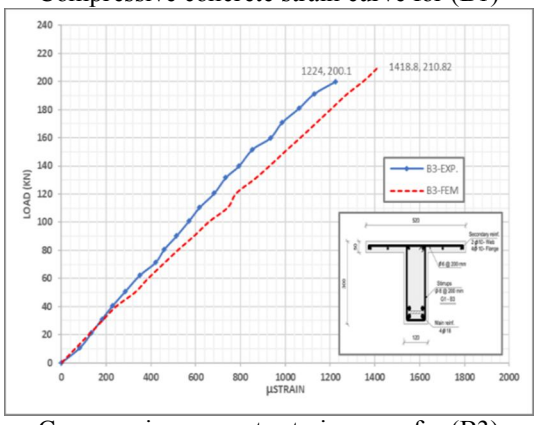

Compressive concrete strain curve for (B3)

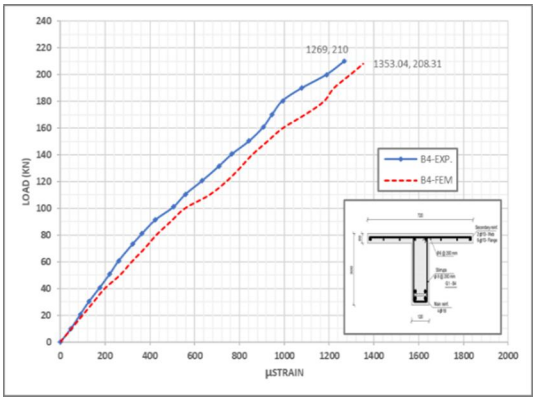

Compressive concrete strain curve for (B4)

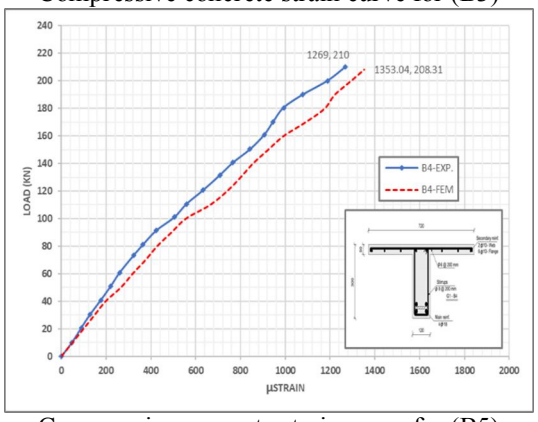

Compressive concrete strain curve for (B5)

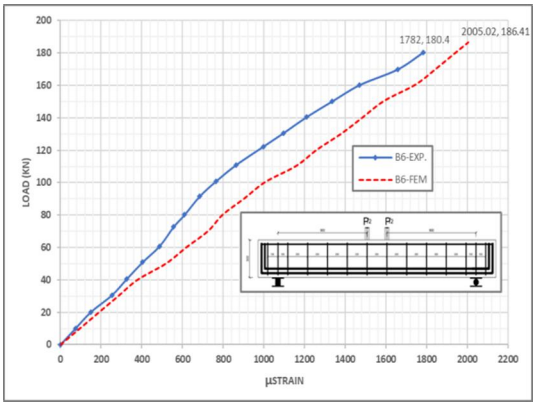

Compressive concrete strain curve for (B6)

Figure 13: Applied load versus compressive concrete strain in the beam specimens.

5 Conclusions

The experimental and theoretical investigations that were carried out in this study led to the following conclusions:

1) No significant difference in the shear behaviour was observed when the flange width was greater than b_w+8T_s, consistent with the flange width recommendation ($Lz_{/5}$ + b) in the Egyptian code.

2) The ultimate load significantly increases with decreasing shear span to depth ratio.

3) In the experimental and FE studies, the failure load of the T-beams with different flange widths (320, 520, and 720 mm) increased with flange width.

4) In the experimental and FE studies, the failure load is inversely proportional to the shear span to depth ratio.

5) In the experimental and FE studies, the vertical deflection, longitudinal steel strain, stirrup steel strain and compressive concrete strain of the T-beams with various flange widths (320, 520, and 720 mm) decreased with increasing flange width.

6) In the experimental and FE studies, the vertical deflection, longitudinal steel strain, stirrup

steel strain and compressive steel strain were directly proportional to the shear span to depth ratio.

7) The ANSYS® program gives an adequate prediction of the shear strength of beams, with average differences of approximately 4.14% in the failure load, 7% in the deflection, 8.42% in the longitudinal steel strain, 14.05% in the stirrup steel strain, and 7.25% in the compressive concrete strain results.

References

1. H. O. Okail, Flexural Behaviour of Reinforced Self-Compacting Lightweight Concrete Beams, Cairo: Ain shams university, 2008.
2. F. Maree and K. H. Riad, "Analytical and experimental investigation for bond behaviour of newly developed polystyrene foam particles," Engineering Structures, vol. 58, 2014.
3. S. A. El Khouly, Behaviour of Foam Particles Lightweight Concrete with Time, Cairo: Ain Shams university, 2016.
4. Tena-Colunga and H. Archundia-Aranda, "Behavior of reinforced concrete haunched beams subjected to static shear loading," Engineering Structures - Elsevier, vol. 30, pp. 478--492, 2008.
5. R. Hawileh, A. Rahman and H. Tabatabai, "Nonlinear finite element analysis and modelling of a precast hybrid beam--column connection subjected to cyclic loads," Applied mathematical modelling - Elsevier, vol. 34, pp. 2562--2583, 2010.
6. R. Hawileh and J. a. T. M. Abdalla, "Modelling of nonlinear response of R/C shear deficient T-beam subjected to cyclic loading," Computers & Concrete - Techno-Press, vol. 10, no. 4, pp. 419-434, 2012.
7. C. M. Foley and E. R. Buckhouse, "Structural Engineering Report MUST-98-1 Strengthening Existing Reinforced Concrete Beams for Flexure Using Bolted External Structural Steel Channels," 1998.
8. "ANSYS. ANSYS User's Manual version 16.0. ANSYS, Inc., Canonsburg".

7/27/2019